



# Radiosensitizing effect of dendrosomal nanoformulation of curcumin on cancer cells

Tahereh Jalali Varnamkhasti<sup>1</sup> · Meisam Jafarzadeh<sup>1</sup> · Majid Sadeghizadeh<sup>1</sup> · Mahdi Aghili<sup>2</sup>

Received: 27 January 2022 / Revised: 17 June 2022 / Accepted: 20 June 2022 / Published online: 10 July 2022  
© The Author(s) under exclusive licence to Maj Institute of Pharmacology Polish Academy of Sciences 2022

## Abstract

**Background** Curcumin was found to possess numerous pharmacological activities in clinical research, however, its biological effects together with radiation are yet to be addressed. The present study investigated whether the combined treatment of dendrosomal nanoformulation of curcumin (DNC) and gamma radiation can enhance the radiosensitivity of U87MG and MDA-MB-231 cell lines.

**Methods** U87MG and MDA-MB-231 cell lines were exposed to 2 Gray (Gy) and 10  $\mu$ M DNC determined by MTT assay, then subjected to clonogenic assay, cell cycle assay, and flow cytometric apoptosis analysis. Acridine Orange/Ethidium Bromide (AO/EB) and 4',6-diamidino-2-phenylindole dihydrochloride (DAPI) stained cells were used to study morphologic changes. The expression evaluation of putative cell cycle genes, i.e., *P53*, *P21*, *CCND1*, and *CCNB1* was carried out by RT-qPCR.

**Results** Our findings indicated that the combined treatment with DNC and radiation might cooperatively augment the efficacy of ionizing radiation in the cancer cells and notably decrease the survival and viability of the cells in a time- and concentration-dependent manner. In addition to a synergistic effect deduced by sensitizer enhancement ratio (SER) assessment, co-treatment resulted in greater apoptotic cells than the individual treatments. Further experiments then indicated that DNC could effectively induce G2/M phase cell cycle arrest and apoptosis following irradiation. Conformably, there was a decrement of *CCND1* and *CCNB1* expression, and an increment of *P53*, *P21* expression.

**Conclusions** The data implied that DNC as a radiosensitizer can enhance the lethal effect of ionizing radiation on cancer cells which could be a promising adjuvant therapy in clinical treatments.

**Keywords** DNC · Gamma radiation · Treatment · Cancer · U87MG · MDA-MB-231

## Abbreviations

AO/EB Acridine orange/ethidium bromide  
Ctrl Control

D Dosage  
DAPI 4',6-Diamidino-2-phenylindole dihydrochloride  
DDR DNA damage response  
DNC Dendrosomal nanoformulation of curcumin  
Eq. Equation  
Gy Gray  
IQR Interquartile range  
IC Inhibitory concentration  
IR Irradiation  
LQ Linear quadratic  
OA Oleic acid  
PE Plating efficiency  
PEG Polyethylene glycol  
PI Propidium iodide  
Q Quartile  
SF Surviving fraction  
SER Sensitizer enhancement ratio

✉ Majid Sadeghizadeh  
sadeghma@modares.ac.ir

✉ Mahdi Aghili  
aghili@sina.tums.ac.ir

Tahereh Jalali Varnamkhasti  
jalali.tah@gmail.com

Meisam Jafarzadeh  
j.meisam68@yahoo.com

<sup>1</sup> Department of Molecular Genetics, School of Biological Sciences, Tarbiat Modares University, P.O. Box 14115-154, Tehran, Iran

<sup>2</sup> Radiation Oncology Research Center, Cancer Institute, Imam Khomeini Hospital Complex, Tehran University of Medical Sciences, P.O. Box 13145-158, Tehran, Iran

## Introduction

Radiotherapy is a mainstay in treating brain and spinal cord tumors [1]. The brain tumor is considered a risk factor for developing gliomas originating from breast cancer, the second most common source of brain metastases [2, 3]. Ionizing radiation can damage DNA leading to cell death directly or indirectly via creating free radicals; however, the efficacy of this approach is limited by the phenomenon termed radioresistance. An entangled network of DNA damage response (DDR), including DNA repair pathways, DNA damage tolerance, and cell-cycle checkpoints plays a critical role in the resistance of cancerous cells after being exposed to ionizing radiation [4, 5]. Based on research findings, irradiation induces a major cell cycle arrest via G1 and G2 phases, which in turn is controlled by the up-regulation of tumor suppressor *P53* and the cyclin-dependent kinase inhibitor *P21*, and its primary downstream target [6, 7]. Curcumin (Diferuloylmethane), a major component of turmeric (*Curcuma longa*) [8, 9], was indicated as a molecule that may exert anti-proliferative effects through its impacts on various biological pathways involved in cell cycle regulation, apoptosis, tumorigenesis, and metastasis [10–13]. Furthermore, it was suggested that the formulation of curcumin in nanoparticles shows a promising therapeutic properties compared to native curcumin [14, 15]. Therefore, to overcome the limitation of curcumin [16, 17], dendrosome was introduced as a biologic and biodegradable nanoscale carrier, since its interior core structure allows the assimilation of hydrophobic curcumin resulting in the enhancement of bioavailability, bioabsorption, and the biological activity of curcumin [18, 19]. According to published research, dendrosomal nanoformulation of curcumin (hence referred to as DNC) can inhibit cancer cell growth and cause apoptosis in vitro and in vivo. Moreover, it may exert its effect by controlling the expression of a large number of genes and non-coding RNAs, consequently regulating epigenetic regulatory processes [20–27]. Upon this background, we assessed the radiosensitizing effects of DNC on brain and breast cancer cell lines after irradiation, then investigated its impacts on the expression of cell cycle and apoptosis regulatory genes. In this regard, U87MG and MDA MB 231 as two types of more invasive and radioresistant cell lines with varying levels of *P53* were used [28, 29].

## Materials and methods

### Cell culture

The human high-grade glioma cell line U87MG and triple-negative breast cancer cell line MDA MB 231 were purchased from the National Cell Bank of Pasteur Institute,

Iran, and grown in Dulbecco's Modified Eagle Medium (Life Technologies, Carlsbad, CA, USA), supplemented with 100 mL/L FBS (Gibco, USA), 100 U/mL penicillin and 100 mg/mL streptomycin (Gibco, USA). They were incubated in a humidified atmosphere (5% CO<sub>2</sub>) at 37 °C and adjusted to expand to the extent of exponential growth.

### Preparation of DNC

Dendrosome, polymeric micelles of oleic acid (OA) and polyethylene glycol 400 (PEG 400), as a carrier (OA400) was obtained from the Institute of Biochemistry and Biophysics, University of Tehran, Iran, and loaded with curcumin (Darmstadt, Germany) by the purity of 95% on the report of optimized weight ratio of 1:25, to gain a maximum ratio of drug loading nanoparticles as described previously [18, 20, 21]. The prepared stock solution was stored in a dark glass bottle at 4 °C, then was diluted to the favorable concentrations by culture medium once for use.

### Cell viability assay

MTT (3-(4, 5-dimethylthiazol-2-yl)-2, 5-diphenyltetrazolium bromide) tetrazolium reduction assay (Sigma-Aldrich, USA) was used to measure the cytotoxic effects of DNC on cell lines. For this purpose, about  $1 \times 10^4$  cells/well, obtained based on the standard curve, were seeded in 96-well plates and allowed to attach overnight. Then, various concentrations of DNC, dendrosome OA400, and curcumin were added to a 10% FBS/DMEM culture medium and incubated for 48 h. Then, the media were removed, and the cells were exposed to 200  $\mu$ L per well of DMEM consisting final concentration of 0.5 mg/ml MTT for up to 3 h at 37 °C in a 5% CO<sub>2</sub> incubator. Then, the media were substituted with 200  $\mu$ L dimethylsulfoxide (Sigma-Aldrich, USA), and the plate was kept in the dark at room temperature for 3 h. Because mitochondrial activity is related to the number of viable cells, the amount of formazan dye (assumed to represent the percentage of living cells) was measured using microplate spectrophotometers (BioTek, ELX 800, USA) based on the optical density of dye solution at 570 nm [30]. Ultimately, the percentage of viable cells was calculated using (Eq. 1); (equation is abbreviated as Eq). In parallel, gamma irradiation was carried out using a source of Cobalt-60 (Theratron 780, Canada) at a dose rate of 100 cGy/min at the Cancer Institute, Tehran University of Medical Sciences, Iran. Control cells were under the same storage condition as irradiated cells. The cells were incubated up to 48 h after treatment, and then the viability assessment was undertaken.

$$\text{Percentage of cell viability (\%)} = \frac{OD\ 570\ \text{treatment}}{OD\ 570\ \text{control}} * 100 \quad (1)$$

To estimate the half-maximal inhibitory concentration (IC<sub>50</sub>) of DNC, a dose–response curve with respect to normalized absorbance was drawn for cells were exposed to 2 Gy at various DNC concentrations.

### Clonogenic survival assay

The plating efficiency (PE) of cells exposed to radiation was determined to estimate their ability for regeneration and reproductive integrity. The proportion of plated cells that differentiate into colony-forming cells is indicative of post-treatment survival. Exponentially growing cells were treated with varying radiation doses, between 0 and 8 Gy in all replicates. In the case of combined treatment, 10 μM DNC (a lower dose than IC<sub>50</sub> value) was added to the cultures 4 h prior to irradiation to ensure that a requisite amount of DNC was absorbed by the cells [31], then treated cancer cells exposed to the defined radiation doses. Forthwith, the appropriate number of cells were harvested and seeded in triplicate into six-well cell culture plates with fresh growth media. The cells were incubated for 1–2 weeks until control plates had formed large clones; colonies of 50 cells or more were considered to have survived the treatment. Then, the colonies were washed with PBS and fixed and stained with 10% formalin (Merck KGaA, Germany) & 0.5% crystal violet (Merck KGaA, Germany) solution, respectively [32, 33]. The plating efficiency of U87MG and MDA-MB-231 cells was determined under the same physiological condition with no treatment and with 10 μM DNC treatment (Eq. 2). Following that, the surviving fraction (SF) (Eq. 3) was calculated as the ratio of surviving colonies to the number of plated cells with correction for the plating efficiency.

$$\text{Plating Efficiency (\%)} = \frac{\text{Number of colonies formed}}{\text{Number of cells seeded}} * 100 \quad (2)$$

$$\begin{aligned} \text{Surviving Fraction (\%)} \\ = \frac{\text{Number of colonies formed after treatment}}{\text{Number of cells seeded} * \text{PE}} * 100 \end{aligned} \quad (3)$$

### Cell cycle assay

Flow cytometry was done to measure the DNA content of the treated cells and make contrast cells in different phases of the cell cycle.  $3 \times 10^6$  cells/well of U87MG and MDA-MB-231 cells were seeded in six-well plates, then treated with the indicated doses as mentioned earlier. After 48 h of incubation, cells were harvested and washed twice with PBS, then fixed in 75% ethanol at 4 °C for 30 min. Henceforth,

the cells were suspended in a cold PBS solution containing 50 μg/mL PI, 0.1% sodium citrate & 0.1 Triton X-100 (Sigma-Aldrich, T8532) lysis buffer and were shaken at 37 °C for 15 min. The distribution of nuclear DNA was examined by analyzing at least  $0.2 \times 10^4$  cells per sample using FACS Calibur™ flow cytometer (BD, NJ) and further processing by FlowJo software [34].

### Flow cytometric apoptosis assay

The double labeling with FITC-Annexin V and propidium iodide (PI) was used to measure the number of cancer cells that had undergone apoptosis. U87MG and MDA-MB-231 cells that were exponentially growing were sown at a density of  $3 \times 10^6$  cells/well in six-well plates overnight, then treated and incubated for 48 h. Cells were stained according to the kit's protocol; in brief, they were labeled with FITC-Annexin V and propidium iodide solution (Roche Applied Science, Penzberg, Germany) and incubated in a binding buffer for 15 min in the dark. Stained cells were immediately analyzed by the FACSCalibur™ flow cytometer (BD, NJ) machine then distribution assessment was accomplished by FlowJo software [35].

### Detection of morphological features of apoptosis and nuclear changes

Differential staining with specific fluorochromes was used to visualize nuclear changes and typical morphological features of apoptosis. For this purpose,  $1 \times 10^4$  cells/well were seeded in 96-well plates and incubated overnight then treated. After 48 h, the plates were centrifuged at 1000 RPM for 5 min, and 100 μl AO/EB dye mix (Sigma, St. Louis, MO, USA) was added to each well. The dye mix contained 5 μg/ml acridine orange and 3 μg/ml ethidium bromide in PBS [36]. Parallel to this experiment, cells were washed twice with PBS and fixed for 20 min with 4% formaldehyde in PBS. For further investigation, the fixed cells were stained with 1 g/ml 4', 6-diamidino-2-phenylindole dihydrochloride (DAPI), Sigma-Aldrich D-8417, and photographed (at 200× magnification) using an Olympus BX51 fluorescent microscope and a DP72 digital camera [35]. The obtained images were then undergone further processes and merged by the software ImageJ, Java 1.8.0\_172 [37]. To indicate the ionizing radiation-induced DNA damage, cytokinesis-block micronucleus assay (CBMN) as the cytogenetic technique was done [38].  $3 \times 10^6$  cells/well were seeded in six-well plates and incubated overnight, then treated. At the time of 44 h, cells were exposed to cytochalasin B (Sigma-Aldrich, USA) up to the final concentration of 6 μg/ml and kept in the incubator for 28 h more. The attached cells were washed with cold PBS and gently treated in a cold (4 °C) 75 mM KCl solution, then fixed with cold methanol and acetic acid (4:1 v/v) for 20 min

**Table 1** Primer sequences for real-time PCR

Genes	Forward primer	Reverse primer
<i>GAPDH</i>	5'-CCGAGCCACATCGCACAG-3'	5'-GGCAACAATATCCACTTTACCAG-3'
<i>p53</i>	5'-CTGAGGTTGGCTCTGACTGTACC-3'	5'-ACACGCACCTCAAAGCTGTTC-3'
<i>p21</i>	5'-ACCAGCATGACAGATTTCTACCA-3'	5'-ACTAAGGCAGAAGATGTAGAGCG-3'
<i>MELK</i>	5'-TTCCCAAGTGGCTCTCTCCAG-3'	5'-TCCTCCATTGTTTGCCTGTTGTTTCT-3'

at 4 °C, (three times), and ultimately were stained with 10% (v/v) Giemsa solution 10% (v/v) (Merck KGaA, Germany) for 10 min. Binucleated cells were observed under Olympus GX51 inverted light microscope (Olympus Corporation, Tokyo, Japan) to see the nuclear anomalies (at 40× magnification): micronuclei; tailed nuclei; nucleoplasmatic bridges; dumbbell-shaped nuclei; etc., as a consequence of chromosomal breakage [39].

### RNA isolation, cDNA synthesis & RT-PCR

After 48-h treatment, total RNA was extracted from treated and untreated cells using Trizol reagent (Life Technologies) according to the manufacturer's instructions, followed by DNase I digestion (Thermo Fisher Scientific, Waltham, MA, USA). For cDNA synthesis, ~1 µg total RNA was reverse-transcribed into cDNA using PrimeScript™ RT reagent kit (Takara Bio Inc, Shiga, Japan). cDNA was stored at -20 °C for PCR. Quantitative PCR (qPCR) was performed using SYBR® Premix Ex Taq™ II (Takara) and specific primers (Table 1) on Applied Biosystems followed by 45 cycles: stage 1, 95 °C for 5 s; stage 2, 60 °C for 20 s; stage 3, 72 °C for 30 s. Relative gene expression was normalized based on *GAPDH* as the reference gene and calculated by  $2^{-\Delta\Delta C_t}$  method [40].

### Statistical analysis

Prism® (GraphPad Software, Inc, La Jolla, CA, USA), version 9.3.1. was used for data analysis. Results are representative of three independent experiments expressed as median with interquartile range (IQR) unless indicated otherwise. Data of clonogenic assay are presented in Bioconductor software (version: 3.11 & R package version 1.22.0) [41]. Statistical significance was assessed using a non-parametric test, one-way ANOVA (Kruskal–Wallis test) followed by Dunn's multiple comparison test; the differences between groups were considered statistically significant if  $p \leq 0.05$  [42].

## Results

### DNC inhibited the viability

The MTT assay was used to analyze the effects of DNC together with gamma on the viability of cancer cells. Prior to

the assay, standard curves of absorbance versus cell density were drawn for both U87MG (Fig. 1A) and MDA-MB-231 (Fig. 1B) cell lines to estimate the optimized cell number with reproducible superior, which was estimated around  $1 \times 10^4$  cells/well in this study. The inhibitory efficacy of DNC and curcumin against cell growth was tested in the same concentration range, and OA400 was employed as a nanoformulated carrier of curcumin to determine if the cytotoxicity of DNC is altered by its carrier. As seen in (Fig. 1C, D), DNC and curcumin reduced cell viability in a time- and concentration-dependent way in both cell lines, but OA400 had no cytotoxicity. Our data demonstrate that DNC has greater inhibitory effect than curcumin; however, no significant differences were observed below 80 µmol/L (Kruskal–Wallis test followed by Dunn's multiple comparison test [ $H(10) = 22.67$ ,  $*p = 0.0120$ ,  $N1-N11 = 3$ ]<sub>Curcumin</sub>, [ $H(10) = 29.37$ ,  $**p = 0.0011$ ,  $N1-N11 = 3$ ]<sub>DNC</sub> for U87MG cells (Fig. 1C); [ $H(10) = 21.18$ ,  $*p = 0.019$ ,  $N1-N11 = 3$ ]<sub>Curcumin</sub>, [ $H(10) = 26.67$ ,  $**p = 0.0029$ ,  $N1-N11 = 3$ ]<sub>DNC</sub> for MDA-MB-231 cells (Fig. 1D)).

Further, cancer cells were exposed to the different radiation doses of gamma (2–8 Gy) and subjected to the assay after 48 h. No-significant differences between control and 2 Gy, and control and 4 Gy were detected (Kruskal–Wallis test followed by Dunn's multiple comparison test [ $H(4) = 13.03$ ,  $***p < 0.0001$ ,  $N1-N5 = 3$ ] for U87MG cells (Fig. 1E); and [ $H(4) = 12.97$ ,  $***p < 0.0001$ ,  $N1-N5 = 3$ ] for MDA-MB-231 cells (Fig. 1F)).

Logarithmically transformed various concentrations of DNC were plotted against normalized absorbance then IC50 was estimated 1.213 µM for U87MG (Fig. 1G) and 1.239 µM for MDA-MB-231 cells (Fig. 1H). The results were converted to non-logarithmic values to define IC50 as 16.33 µmol/L and as 17.34 µmol/L for the cells, respectively.

### DNC demonstrated the radiosensitivity & synergistic effect

The radiosensitivity of the irradiated cells treated with 10 µM DNC was assessed by clonogenic survival assay. Radiation dose-survival curves were plotted for U87MG (Fig. 2A) and MDA-MB-231 (Fig. 2B) cell lines and deduced that survival of the cells treated with DNC was lower than respective untreated cells. The linear-quadratic (LQ) equation (Eq. 4) describes the chance of a cell



surviving a single dose of radiation, where SF is the survival percentage and  $D$  is the exposure dose. Radiation survival curves present the data predicted with the linear-quadratic model, and  $\alpha$  and  $\beta$  components are parameters describing the radiosensitivity as  $\alpha$  reflects single hit damage while the  $\beta$  represents multiple hits. The  $\alpha/\beta$  ratio is representative of a value in Gy at which the linear  $\alpha$  and quadratic  $\beta$  contributions are equal; hence a high  $\alpha/\beta$  ratio indicates more sensitivity with increasing dose [43, 44]. The sensitizer enhancement ratio or SER (Eq. 5) was defined as the ratio of the radiation dosage ( $D$ ) necessary to decrease the survival fraction to 50% in the absence of sensitizer to the dose required to achieve the same survival fraction with sensitizer [45]. SER value higher than 1.20 indicates radiosensitization.

$$SF = e^{-(\alpha D + \beta D^2)} \quad (4)$$

$$SER = D_{50}(\text{irradiation})/D_{50}(\text{irradiation \& DNC}) \quad (5)$$

The radiosensitization effect of DNC treatment on U87MG and MDA-MB-231 cell lines was evaluated using the formulas (Eq. 6), according to Valeriote and Lin (1975), and Carpentier (1993) [46, 47].  $SF_R$  is the surviving fraction of the cells treated by radiation alone, and  $SF_{DNC}$  is the surviving fraction of the cells treated with DNC alone.  $SF_{R+DNC}$  has presented the surviving fraction of the cells treated by DNC and gamma.

Synergism :  $SF_{R+DNC} < SF_R * SF_{DNC}$

Additivity :  $SF_{R+DNC} = SF_R * SF_{DNC}$

Sub-additivity :  $SF_{R+DNC} > SF_R * SF_{DNC}$ , with  $SF_{R+DNC} < SF_R$  and  $SF_{R+DNC} < SF_{DNC}$

Antagonism :  $SF_{R+DNC} > SF_R$  and/or  $SF_{R+DNC} > SF_{DNC}$

The results are presented in Tables 2, 3, indicating that DNC might attribute sensitivity to radiation in U87MG and MDA MB 231 cells and induce decreased survival of cancer cells compared to radiation alone. In our study, the effect of DNC at various doses of radiation was found synergistic and radiosensitizer.

### DNC triggered cell cycle G2/M arrest

Flow cytometric analysis results depicted the accumulation of treated cells in different phases of the cell cycle after 48 h of treatment for both cell lines (Fig. 3A, B). Statistical analysis revealed that DNC may effectively induce G2/M arrest (Kruskal–Wallis followed Dunn's post hoc test [ $H(3) = 6.0$ ,  $p = 0.0667$ ,  $N1-N4 = 2$ ]<sub>G0/G1</sub>, [ $H(3) = 4.833$ ,  $p = 0.1714$ ,

$N1-N4 = 2$ ]<sub>G2/M</sub> for U87MG cells (Fig. 3C); [ $H(3) = 6.167$ ,  $*p = 0.0381$ ,  $N1-N4 = 2$ ]<sub>G0/G1</sub>, [ $H(3) = 6.0$ ,  $p = 0.0667$ ,  $N1-N4 = 2$ ]<sub>G2/M</sub> for MDA MB 231 (Fig. 3D)).

### DNC induced apoptosis in irradiated cells

To find whether the growth inhibitory effect of DNC and gamma was associated with apoptosis, U87MG (Fig. 4A) and MDA MB 231 (Fig. 4B) cells were incubated with Annexin V-FITC/PI and analyzed by flow cytometry. Cells showing up as Annexin V-/PI+ were of dead cells (Q1). The cells were as lately (Q2) and early (Q3) apoptotic cells were taken Annexin V+/PI+ and Annexin V+/PI-, respectively, whilst the (Q4) quadrant represents viable cells (Annexin V-/PI-). When DNC was used with gamma radiation, the fraction of apoptotic cells (early and late apoptotic cells) was greater than when DNC was used or gamma (Kruskal–Wallis test followed by Dunn's multiple comparison test [ $H(3) = 5.167$ ,  $p = 0.1619$ ,  $N1-N4 = 2$ ]<sub>Dead</sub> for U87MG cells (Fig. 4C); [ $H(3) = 6.452$ ,  $*p = 0.0190$ ,  $N1-N4 = 2$ ]<sub>Alive</sub>, [ $H(3) = 6.167$ ,  $*p = 0.0381$ ,  $N1-N4 = 2$ ]<sub>Early Apoptotic</sub>, [ $H(3) = 5.5$ ,  $p = 0.1143$ ,  $N1-N4 = 2$ ]<sub>Dead</sub> for MDA MB 231 cells (Fig. 4D)). The post hoc comparisons confirmed that DNC and gamma co-treatment resulted in an increased number of dead cells as compared to DNC or irradiation alone.

### Microscopy revealed morphological nuclear changes in apoptotic cells

Differential staining of U87MG cells after 48 h of exposure to 10  $\mu$ M DNC and 2 Gy gamma radiation with DAPI and AO/EB dyes visualized morphological hallmarks of apoptosis. AO can penetrate the membrane of live cells; thus, these cells have circular nuclei in the center with green organized chromatin structures. EtBr which penetrated the cells with damaged membranes represented apoptotic or dead cells with orange-red fluorescence nucleus and condensed or fragmented chromatin structures. Cells with fragmented bright green nuclei or crescent-shaped condensed chromatin represented early

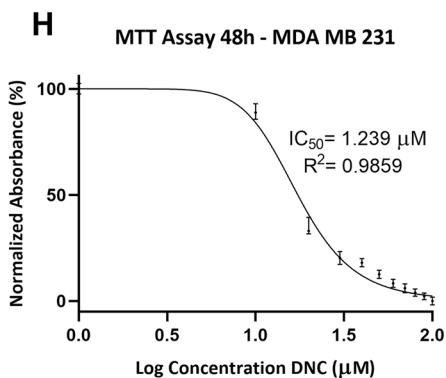
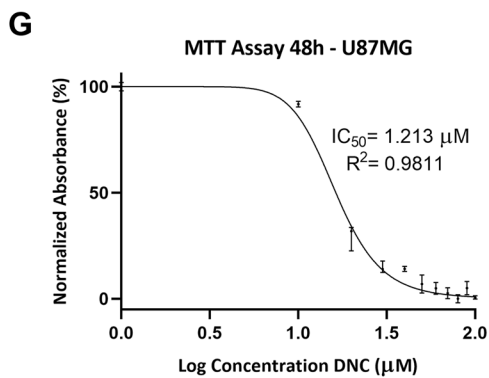
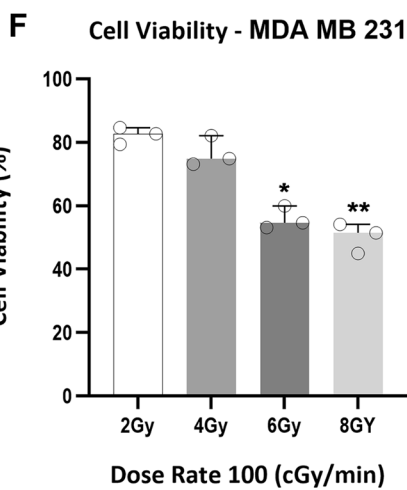
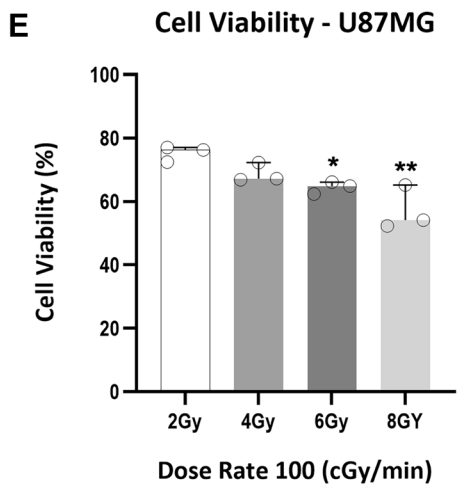
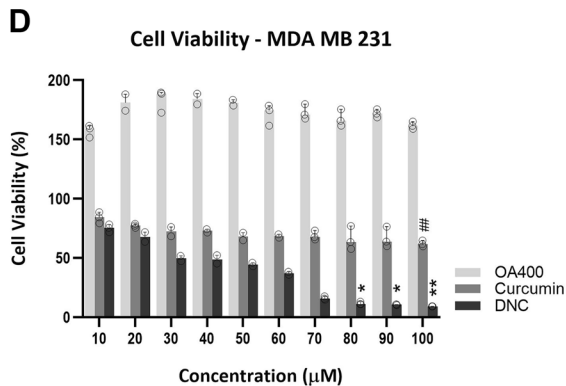
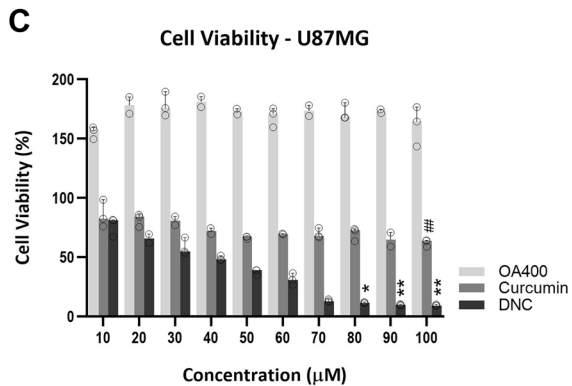
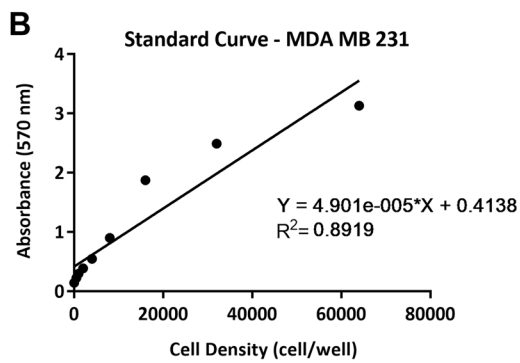
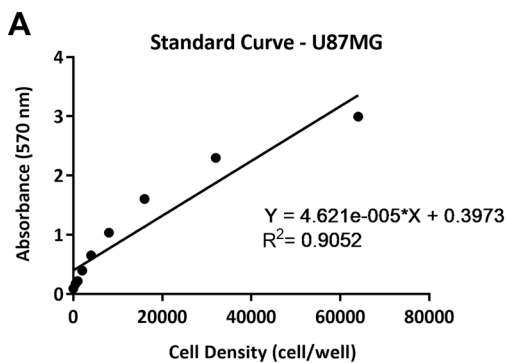


**Fig. 1** DNC affected the viability of the cancer cells. Standard curve of absorbance versus cell density. *X* indicated the optimum number of cells per well relating to absorbance on the *Y*-axis; (A)  $R^2=0.9052$ , (B)  $R^2=0.8919$ . Toxicity effects of OA400, Curcumin, and DNC. Cells were subjected to different concentrations (10–100  $\mu\text{mol/L}$ ) of curcumin, DNC (dendrosomal nanoformulation of curcumin), and OA400 (Oleic Acid) for 48 h. Kruskal–Wallis test followed Dunn's post hoc test: (C) \*  $p_{80\mu\text{M}}=0.0225$ ; \*\*  $p_{90\mu\text{M}}=0.0075$ ; \*\*  $p_{100\mu\text{M}}=0.0023$ ; ##  $p_{100\mu\text{M}}=0.0062$ , (D) \*  $p_{80\mu\text{M}}=0.046$ ; \*  $p_{90\mu\text{M}}=0.010$ ; \*\*  $p_{100\mu\text{M}}=0.002$ ; ##  $p_{100\mu\text{M}}=0.0066$ . As the viability of the control group was considered 100%, its data are not depicted but considered in the statistical calculation. (N1–N11=3). Toxicity effect of Gamma radiation. Cells were subjected to various dosages of Gamma (2–8 Gy (Gray)—dose rate: 100 centigray per minute) for 48 h. Kruskal–Wallis test followed Dunn's post hoc test: (E) \*  $p=0.0325$ ; \*\*  $p=0.0076$ , (F) \*  $p=0.0423$ ; \*\*  $p=0.0056$ . As the viability of the control group was considered 100%, its data are not depicted but considered in the statistical calculation. (N1–N5=3). Toxicity effect of combined treatment of DNC and Gamma. Cells were exposed to 2 Gy of gamma radiation and various dosages of DNC. All concentrations are provided as logarithmically transformed values against the normalized quantity of absorbance in dose–response curves. (G)  $\text{IC}_{50}=1.213 \mu\text{M}$ , (H)  $\text{IC}_{50}=1.239 \mu\text{M}$ ;  $\text{IC}_{50}$ : half-maximal inhibitory concentration

apoptotic cells, and orange nuclear-fragmented bodies resulting from nuclear shrinkage were of late apoptosis. The findings of fluorescence microscopy showed apoptotic morphological characteristics such as cell shrinkage, membrane blebbing, chromatin condensation, nuclear fragmentation, and apoptotic bodies (Fig. 5A). Binucleated cells with the integrity of chromosomes during division represented the intact cells whereas treated cells out of DNA damages exhibited varied abnormal nuclear morphologies: micronuclei; nucleoplasmic bridge; nuclear bud; and tail have appeared after treatment which postulated as unusual forms of nuclear in the dividing cells (Fig. 5B).

### DNC altered expressions of cell cycle genes

The expression analysis of genes involved in proliferation and cell death (*P53*, *P21*, *CCND1*, and *CCNB1*) was performed to further elucidate the effects of the treatment at the molecular level. It was shown that the combined treatment with DNC and gamma radiation can induce increased expression of *P53* and *P21* genes and decreased expression of *CCND1* and *CCNB1* genes compared to the untreated group (Kruskal–Wallis followed Dunn's post hoc [ $H(3)=10.66$ , \*\* $p=0.0024$ , N1–N4=4] $_{P53}$ , [ $H(3)=12.25$ , \*\*\* $p=0.0002$ , N1–N4=4] $_{P21}$ , [ $H(3)=9.470$ , \*\* $p=0.0078$ , N1–N4=4] $_{CCND1}$ , [ $H(3)=8.754$ , \* $p=0.0164$ , N1–N4=4] $_{CCNB1}$  for U87MG (Fig. 6A); [ $H(3)=13.25$ , \*\*\*\* $p<0.0001$ , N1–N4=4] $_{P53}$ , [ $H(3)=11.44$ , \*\* $p=0.0011$ , N1–N4=4] $_{P21}$ , [ $H(3)=9.392$ ,

\*\* $p=0.0060$ , N1–N4=4] $_{CCND1}$ , [ $H(3)=7.948$ , \* $p=0.0306$ , N1–N4=4] $_{CCNB1}$ ) for MDA MB 231 cells (Fig. 6B).

## Discussion

In recent decades, many studies have been done on the possible use of phytochemicals as radiosensitizers to improve the radiotherapeutic efficacy [48]. The importance of turmeric in medicine has been raised with the discovery that the dried rhizome of *Curcuma longa* is highly rich in phenolic compounds described as curcuminoids which exhibit therapeutic activity against a number of diseases, which is attributed to the main active ingredient of turmeric, curcumin [49]. Curcumin (diferuloylmethane), the natural yellow pigment of turmeric, has been extensively studied, and there is evidence that it can enhance the lethal effects of radiation and attenuate the withstanding effects of ionizing radiation in both models, in vitro and in vivo by a multifaceted mechanism on the suppression of survival and induction of cell death pathways [50].

From a clinical standpoint, the primary concern related to radiotherapy is to minimize harm to surrounding normal tissues. Using a radiosensitizer can raise the death rate of cancer cells while also lowering the risk of injury and adverse effects from radiation, since the required dosage can be lowered. Targeting DNA damage response [51], pro-survival signaling pathways [52], tumor hypoxia stat [53], and cell cycle progression [54] are the regular strategies for the development of radiotherapy efficacy and radiation sensitizers.

We assessed the radiosensitizing effects of DNC on human brain cancer cell line U87MG (*P53* wild type) and human breast cancer cell line MDA-MB-231 (*P53* mutant) and investigated whether it affects cell cycle progression and DNA damage-induced apoptosis after irradiation. Our findings demonstrated that DNC has radiosensitivity effects on cancer cells through increasing apoptosis and cell death rate, simultaneously decreasing cell viability and survival, culminating in cell cycle arrest following DNA damage and modifying the expression of some gatekeeper genes. Moreover, the therapeutic application of DNC following radiation was investigated and it was suggested it may behave as a radioprotective agent in combination with ionizing radiation in a dose-dependent manner [55, 56].

The results of the MTT assay showed a growth inhibitory effect of DNC on U87MG and MDA-MB-231 cell lines that are strongly associated with the duration of treatment, concentration, and the formulation used for curcumin delivery. Supportively, other studies indicate that curcumin formulation could improve its efficacy, bioactivity, and bioavailability [17, 57]. OA400 as the nano-carrier of curcumin in the formulation of DNC had no cytotoxic effect on the viability of the cells; on the contrary, it augmented the proliferation

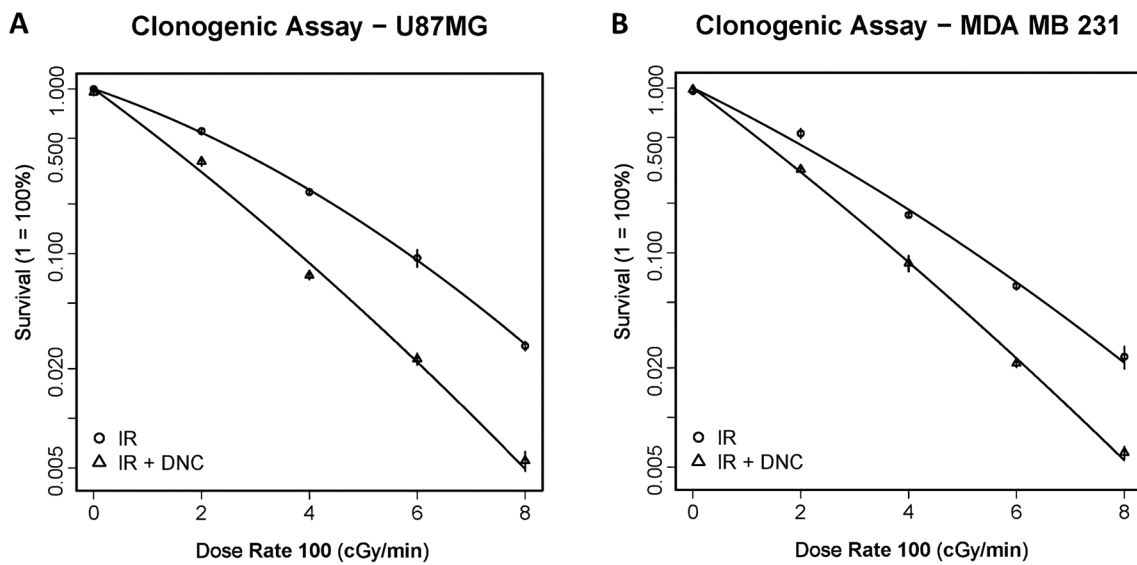


**Fig. 2** DNC affected the surviving fraction in induced gamma cancer cells. Clonogenicity potential of the treated cells. Cells were treated with DNC (10  $\mu\text{mol/L}$ ) for 4 h, then exposed to gamma rays (2, 4,

6, and 8 Gy—dose rate: 100 centigray per minute). Survival curves are representative of irradiated (IR) and DNC treated & irradiated (IR + DNC) groups of (A) U87MG cells, (B) MDA-MB-231 cells

**Table 2** Survival fraction of U87MG and MDA MB 231 cells

Radiation (Gy)	U87MG cells			MDA MB 231 cells		
	SF <sub>R</sub>	SF <sub>R+DNC</sub>	SF <sub>R</sub> * SF <sub>DNC</sub>	SF <sub>R</sub>	SF <sub>R+DNC</sub>	SF <sub>R</sub> * SF <sub>DNC</sub>
2	0.553814	0.362262	0.527921	0.530592	0.320271	0.519879
4	0.236294	0.073755	0.225246	0.169401	0.086370	0.165980
6	0.094067	0.022894	0.089669	0.062932	0.021308	0.061661
8	0.027480	0.005516	0.026195	0.023332	0.006119	0.022860

**Table 3** The effect of 10  $\mu\text{M}$  DNC combined with Gamma radiation

Cell lines—treatment	$\alpha$ (Gy. <sup>-1</sup> )	$\beta$ (Gy. <sup>-2</sup> )	$\alpha/\beta$ ratio (Gy)	SF2	SER (SF = 50%)
U87MG—R	0.259553	0.023342	11.119569	0.553814	1.83
U87MG—R & DNC	0.553673	0.013860	39.947546	0.362262	
MDA MB 231—R	0.369579	0.013824	26.734592	0.530592	1.47
MDA MB 231—R & DNC	0.566788	0.010506	53.948981	0.320271	

of the treated cells. The likely explanation is that OA400 is derived from oleic acid and may cause cell membrane extension during cell division. The observed inhibitory effect of treatment was found because of DNC or curcumin induction in which the effect of DNC was greater than curcumin with the same or higher concentration. However, in the present study, the proper statistical analysis was impossible due to a small sample size; therefore, some statistical effects may be underestimated. Although the concentration of DNC used in this research was lower than the determined IC50 value, our findings suggest that DNC could sensitize U87MG and MDA MB 231 cancer cells and decrease their survival when it is used jointly with 2 Gy of gamma radiation. The ability of a single cell to grow into a colony of cells, measured by

clonogenic assay, is the principal endpoint in radiobiology. Survival probability analysis revealed that DNC might operate as a sensitizer enhancer after radiation. The calculation of sensitizer enhancement ratio (SER) in D50 (SF = 50%) then confirmed that DNC treatment attributed the SER = 1.83 to the irradiated U87MG cells and the SER = 1.47 to the irradiated MDA MB 231 cells which both are greater than indicative radiosensitization index (SER = 1.2).

The quantitative and morphological assessment of annexin V-FITC/PI staining, DAPI, and AO/EB staining indicated the induction of apoptosis in both cell lines, considerably in U87MG cells. P53 is a master regulator gene in the maintenance of cellular genetic integrity, which is reported to be mutated in over 50% of cancer types resulting



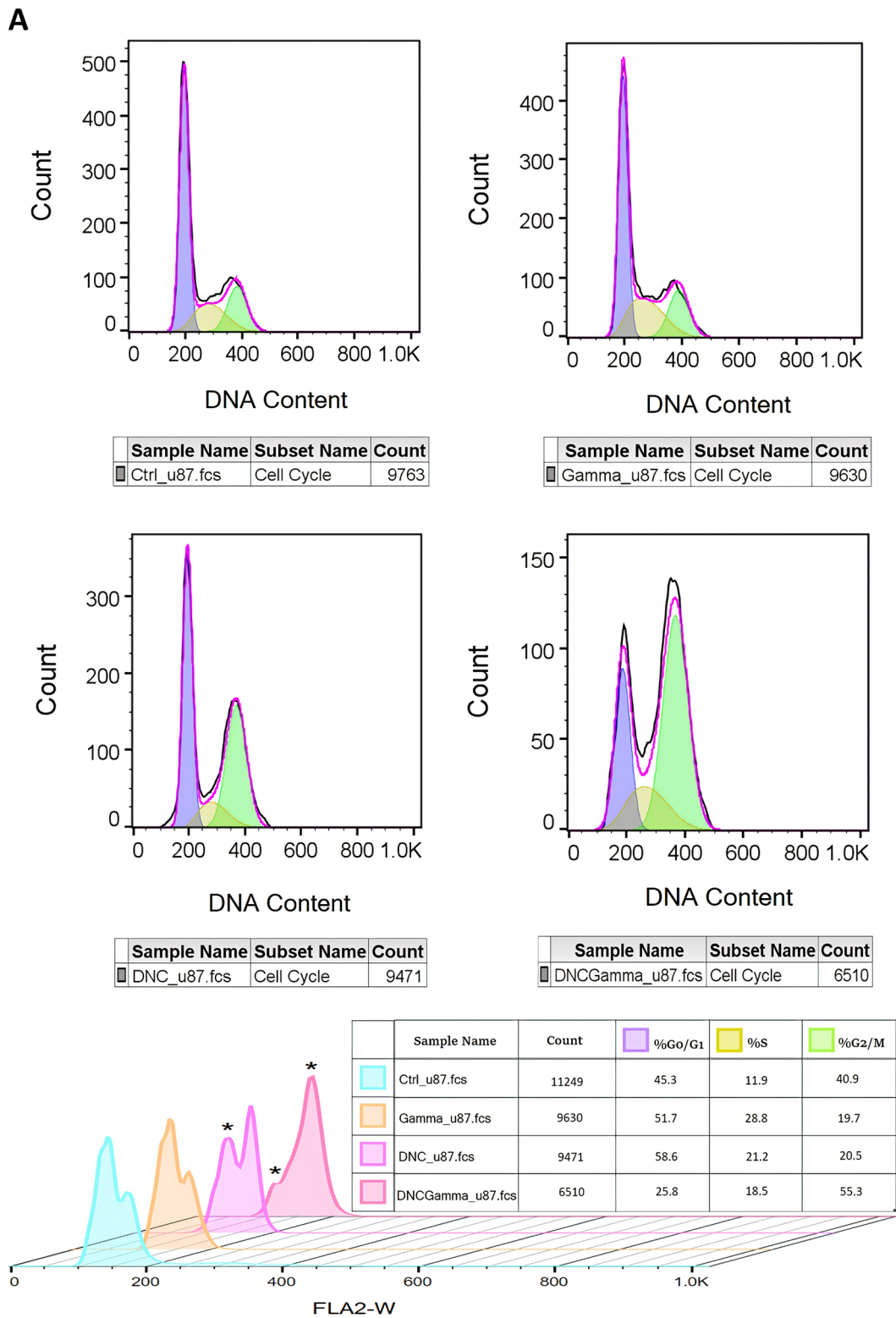


**Fig. 3** Flow cytometry analysis of cell cycle. Histograms of the cell cycle. Distributed ratios of cells of different samples: Control (Ctrl), Gamma, DNC, DNCGamma in G0/G1, S, and G2/M cycles. (A) DNA content distribution of U87MG cells, (B) DNA con-

tent distribution of MDA-MB-231 cells. Analysis of cell cycle. The average percentage of cell count in G0/G1, S, and G2/M cycles. Kruskal–Wallis test followed Dunn's post hoc test: (C)  $*p=0.0412$ ;  $\#p=0.0412$ , (D)  $*p=0.0247$ ;  $\#p=0.0412$ . (N1–N4=2)

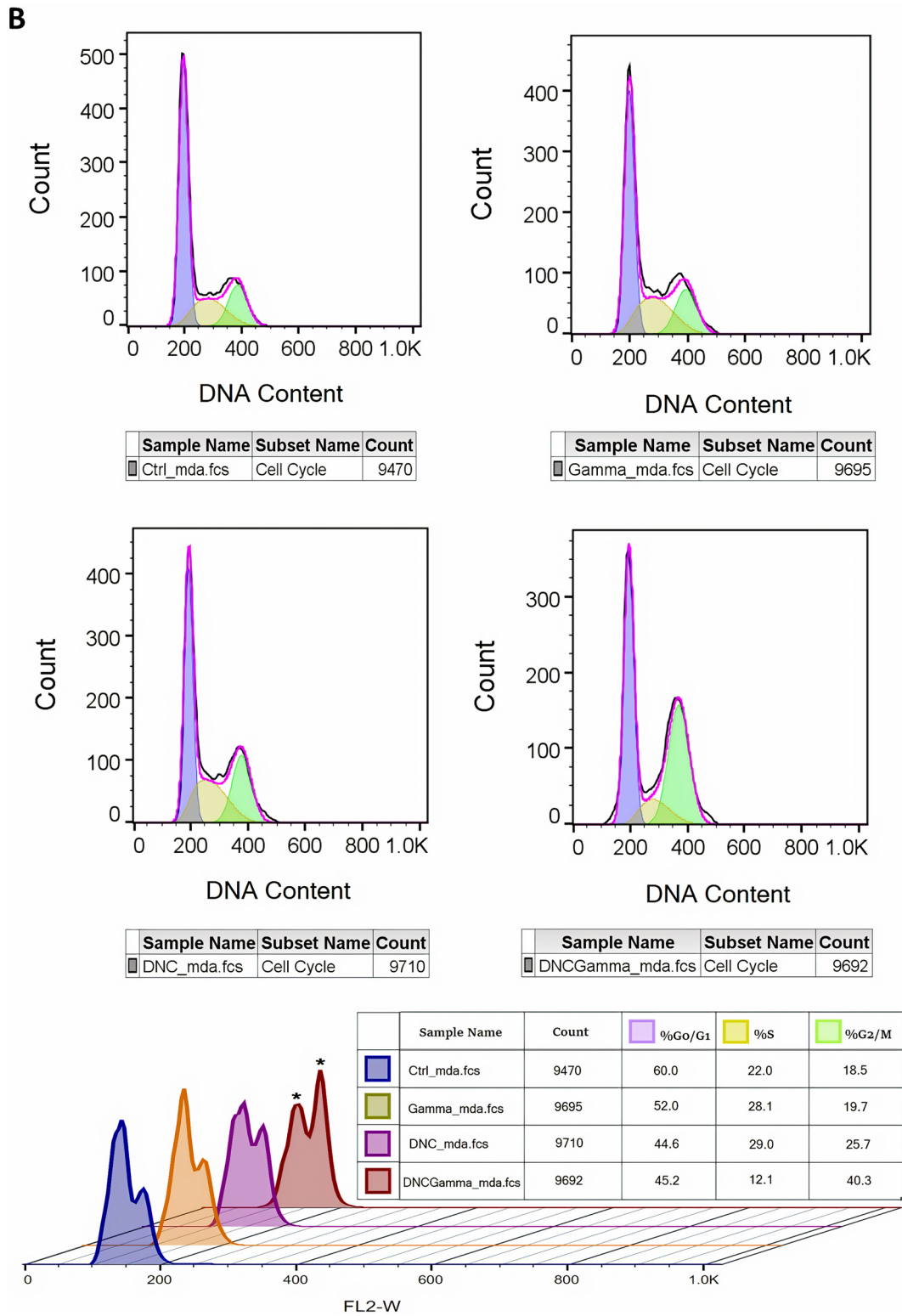


Fig. 3 (continued)

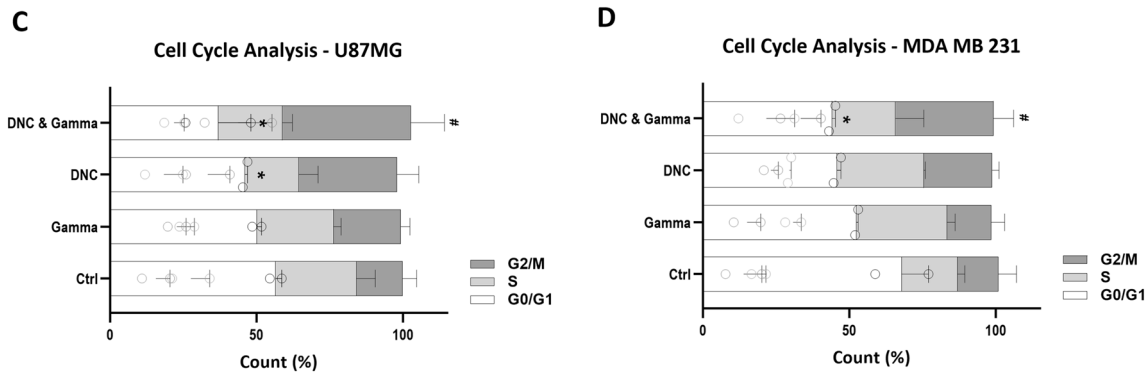


Fig. 3 (continued)

in resistance to apoptosis and sustained proliferation. This gene is involved in various cellular processes, including apoptosis, cell cycle arrest, and DNA repair [58].

DNC treatment was capable of causing a cell cycle arrest at the G2/M phase and trigger apoptosis in the U87MG cell line. It has been evidenced previously that antitumor activity of curcumin is related to its ability to induce G2/M cell cycle arrest and cell death since was already reported via FoxO1 [59], and Wnt [60] signaling pathways, through induction autophagy (self-degradative process) by inhibition of the Akt/mTOR/p70S6K pathway and activation of the ERK1/2 signaling pathway [61], by suppressing the PI3K/AKT and NF- $\kappa$ B/COX-2 signaling pathways [62], through up-regulation of *DUSP-2* expression and inhibition of ERK and JNK phosphorylation [63], by activation of *Bcl-2*-mediated G2 checkpoint [64], through influencing NF- $\kappa$ B, UPR, and Akt/Notch pathways [65], and via interfering with SHH/GLI1 signaling [66] in U87MG cells.

In MDA MB 231 cells, DNC treatment induced a cell cycle arrest in the G2/M phase and began the cell death process. This effect has been previously attributed to autophagy-dependent Akt degradation in PI3K/Akt signaling pathway [67], inhibition of *EGFR* expression [68], silencing *EZH2* and restoring *DLCL1* expression [69], decreasing of *CDC25* and *CDC2* and increasing of *P21* protein levels, as well as inhibition of the phosphorylation of Akt/mTOR [70], deregulating the expression of *cyclin D1*, *PECAM-1*, and *P65*, which are regulated by NF- $\kappa$ B [71], inhibiting Skp2-mediated *P27* ubiquitination in Her2/Skp2-overexpressing cancer cell lines [72], down-regulating *Bcl-2* level while up-regulating *Bax*, cleaved-caspase3 and PARP levels [73] in MDA-MB-231 cells.

Supportively, our data showed that DNC and gamma treatment could up-regulate the expression of *P53* and *P21* and down-regulate the expression of *CCND1* and *CCNB1* genes. One of the main functions of *P53* is controlling DNA replication in response to DNA damage by regulating *p21* protein through the activation of the P53-P21 pathway [74], or independently [75]. Consistent with our findings, it was identified that curcumin can up-regulate apoptosis-inducing genes such as *P53* and *P21* [76], and down-regulate pro-survival genes such as *cyclin D1* [77], and *cyclin B1* [78].

Further assessments such as DNA repair assays are suggested to examine the effects of DNC treatment before or after irradiation. The findings of the present research should be interpreted with caution, not only because of the small size of the study that made the correct statistical analysis deduction impossible, but also because of the limited number of studied cell lines that is not large enough to generalize the effects and results.

## Conclusions

The study shows that DNC may enhance the damaging effects of gamma radiation on cancer cells when used as a radiosensitizer. Regarding the elucidated antioxidative, anti-inflammatory, and anticancerous effects of curcumin and its safe application and low cost, DNC might be figured as a promising adjuvant agent to augment radiotherapeutic efficacy in the treatment of various malignancies.

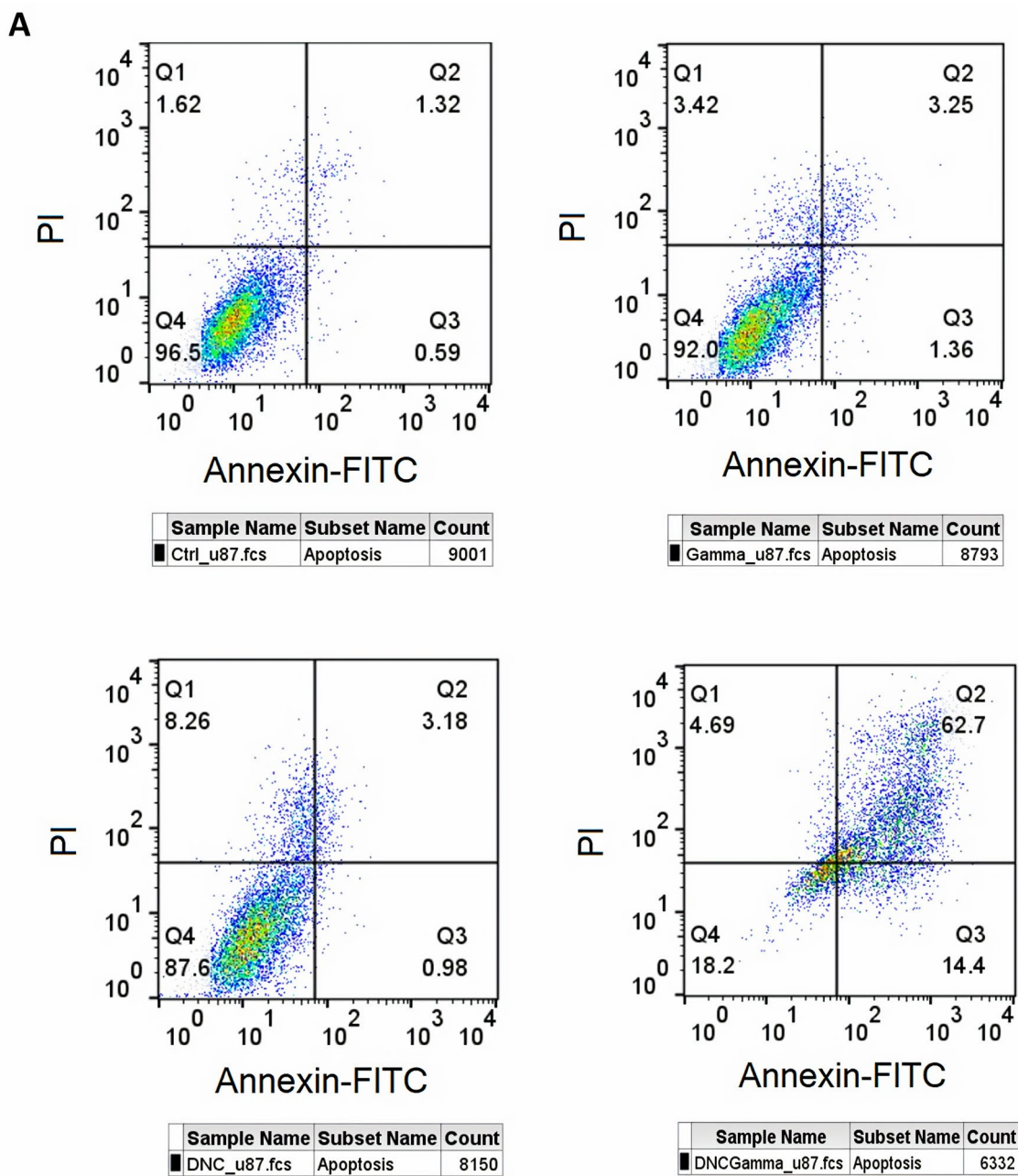
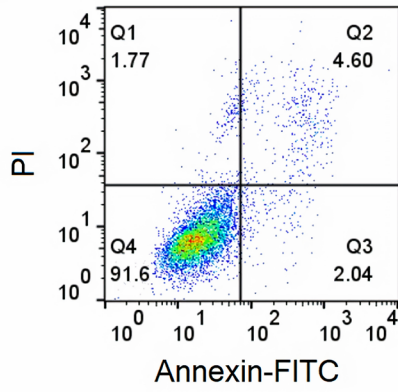


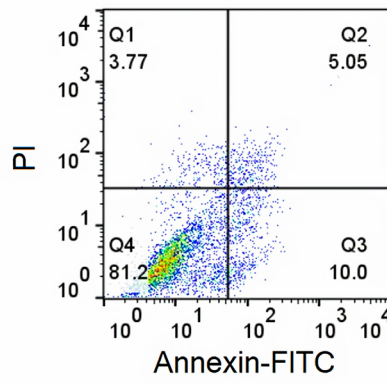
**Fig. 4** Flow cytometry analysis of apoptosis. Histograms of apoptosis. Apoptosis ratios of cells of different samples: Control (Ctrl), Gamma, DNC, DNCGamma in different quartiles (Q): Q1 quadrant represents dead cells (PI+ & Annexin-); Q2 quadrant shows cells that are in late apoptosis (PI+ & Annexin+); Q3 quadrant represents cells in early apoptosis (PI- & Annexin+); Q4 quadrant is the indica-

tive quadrant for viable cells (PI- & Annexin-). (A) DNA content of U87MG cells, (B) DNA content of MDA-MB-231 cells. Analysis of apoptosis. The average percentage of alive (Q4), apoptotic (Q3), and dead (Q1+Q2) cells. Kruskal–Wallis test followed Dunn's post hoc test: (C) <sup>#</sup>*p*=0.0247, (D) <sup>\*</sup>*p*=0.0137; <sup>§</sup>*p*=0.0247; <sup>#</sup>*p*=0.0247. (N1–N4=2)

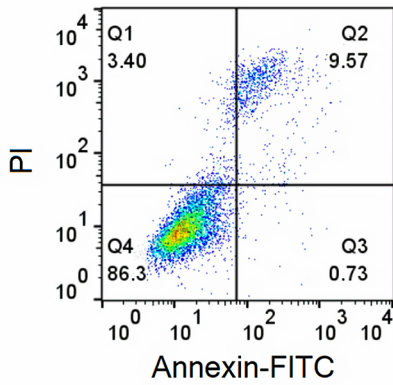
**B**



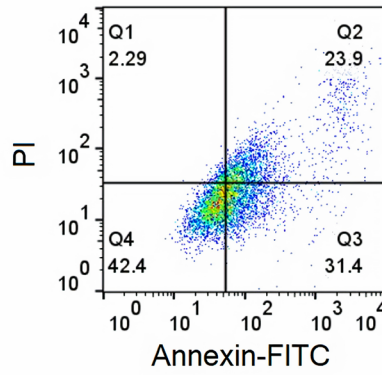
Sample Name	Subset Name	Count
Ctrl_mda.fcs	Apoptosis	8517



Sample Name	Subset Name	Count
Gamma_mda.fcs	Apoptosis	5627



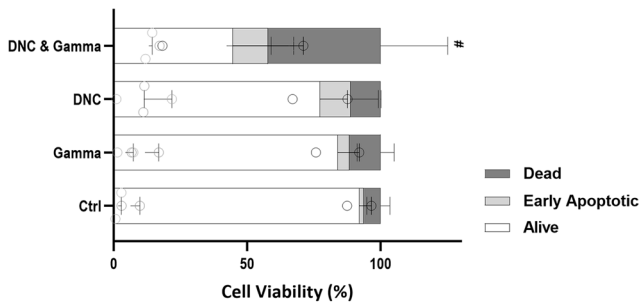
Sample Name	Subset Name	Count
DNC_mda.fcs	Apoptosis	8409



Sample Name	Subset Name	Count
DNCGamma_mda.fcs	Apoptosis	7981

**C**

Cell Apoptosis Analysis - U87MG



**D**

Cell Apoptosis Analysis - MDA MB 231

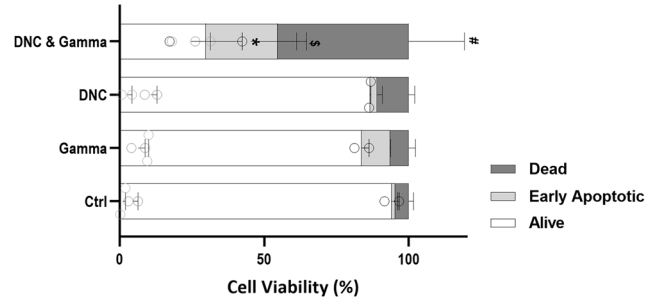
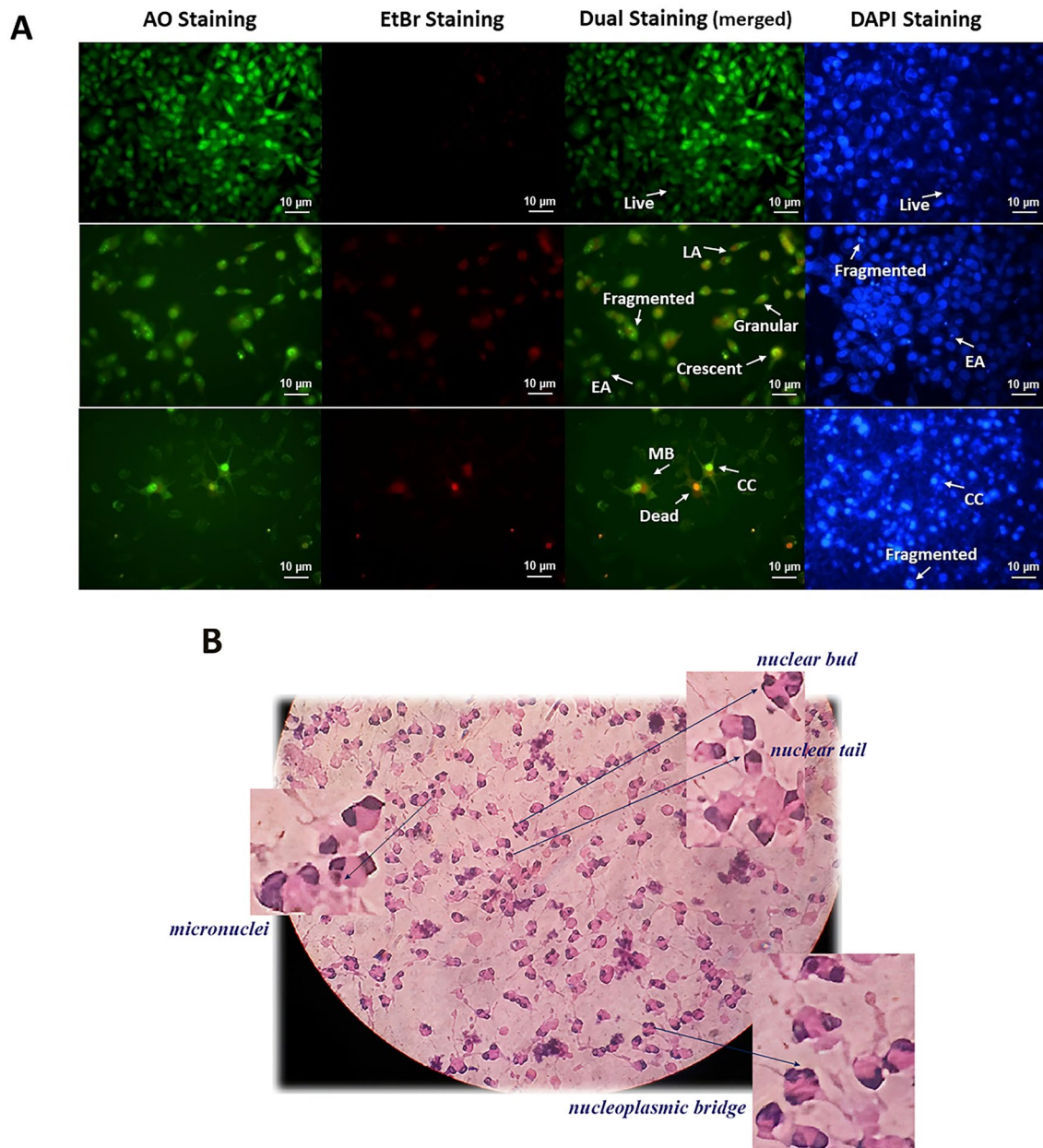


Fig. 4 (continued)

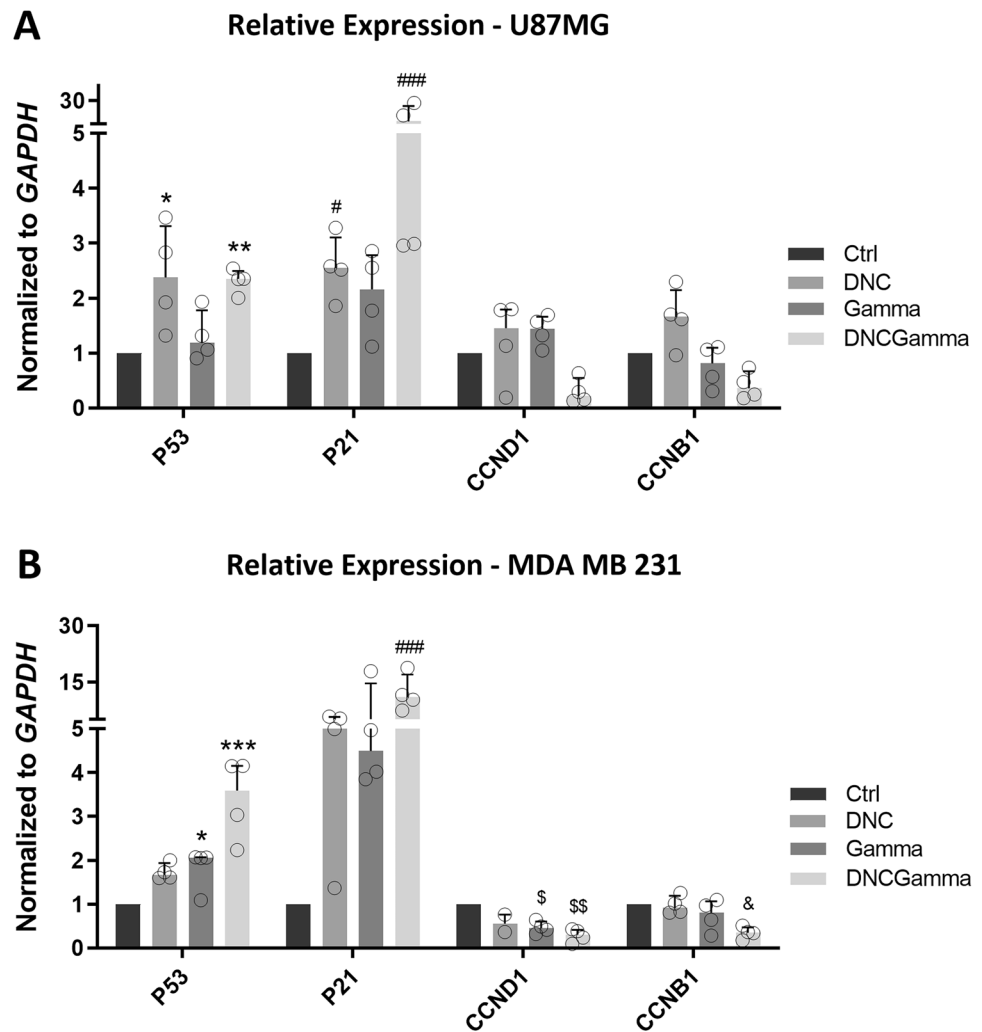




**Fig. 5** Cell and nuclear morphological changes of apoptotic cells. Dual AO/EB staining & DAPI staining. **(A)** Live cells; green circular organized chromatin structures, early apoptotic (EA) cells; yellowish-green crescent-shaped or granular bright green nuclear on one side, late apoptotic (LA) cells; orange nucleus with condensed or fragmented chromatin structures, dead cells; orange-red condensed chromatin structures. Morphological changes of late apoptosis are

marked as membrane blebbing (MB) and chromosome condensation (CC). Olympus GX51 inverted microscope (40×). **(B)** Micronuclei; a biomarker of chromosome breakage or loss, nucleoplasmic bridge; a biomarker of DNA misrepair or telomer end-fusions, nuclear bud; a biomarker of elimination of amplified DNA or DNA repair complexes [79], and nuclear tail; a biomarker of the nuclei protrusion into the cytoplasm owing out of dicentric chromosomes [80]

**Fig. 6** Expression analysis of cell cycle and apoptosis marker genes. RT-qPCR expression analysis of *p53*, *p21*, *CCND1*, and *CCNB1*. *GAPDH* was used as an internal control for normalization of the genes in different samples: Control (Ctrl), Gamma, DNC, DNCGamma. Kruskal–Wallis test followed Dunn's post hoc test: (A) \* $p=0.0110$ ; \*\* $p=0.0071$ ; # $p=0.0300$ ; ## $p=0.0006$ , (B) \* $p=0.0362$ ; \*\*\* $p=0.0003$ ; ### $p=0.0008$ ; § $p=0.0403$ ; §§ $p=0.0028$ ; & $p=0.0136$ . (N1–N4=4)



**Acknowledgements** This project would not have been possible without the support and funding from the Tarbiat Modares University and the Cancer Institute. We thank our colleagues from the radiation oncology department who greatly assisted this paper, particularly Ms. Esfahani and Mr. Nosrati for their notable comments and favors, which made the radiation part of the project possible. Also, the authors would like to thank the anonymous reviewers for their insightful suggestions and careful reading of the manuscript.

**Authors contributions** TJ and MJ performed the measurements and processed the experimental data and statistical analysis. TJ drafted the manuscript and designed the figures. MS and MA were involved in planning, supervising the work, and verifying the numerical results of all experiments. All authors discussed the results and commented on the manuscript.

**Funding** The authors disclosed receipt of the following financial support for the research: This research was supported by a grant from the Vice-Chancellor of Research & Technology of Tarbiat Modares University; and the Cancer Institute, Imam Khomeini Hospital Complex, Tehran University of Medical Sciences.

**Data availability** The data that support the findings of this study are available as Supplementary files.

## Declarations

**Conflict of interest** We know of no conflicts of interest associated with this publication, and there has been no significant financial support for this work that could have influenced its outcome. As the corresponding author, I confirm that the manuscript has been read and approved for submission by all the named authors.

## References

1. Brown PD, Ahluwalia MS, Khan OH, Asher AL, Wefel JS, Gondi V. Whole-brain radiotherapy for brain metastases: evolution or revolution? *J Clin Oncol.* 2018;36(5):483.
2. Darlix A, Louvel G, Fraisse J, Jacot W, Brain E, Debled M, et al. Impact of breast cancer molecular subtypes on the incidence, kinetics and prognosis of central nervous system metastases in a large multicentre real-life cohort. *Br J Cancer.* 2019;121(12):991–1000.
3. Korja M, Raj R, Seppä K, Luostarinen T, Malila N, Seppälä M, et al. Glioblastoma survival is improving despite increasing incidence rates: a nationwide study between 2000 and 2013 in Finland. *Neuro Oncol.* 2019;21(3):370–9.

4. Pearl LH, Schierz AC, Ward SE, Al-Lazikani B, Pearl FM. Therapeutic opportunities within the DNA damage response. *Nat Rev Cancer*. 2015;15(3):166–80.
5. Pilié PG, Tang C, Mills GB, Yap TA. State-of-the-art strategies for targeting the DNA damage response in cancer. *Nat Rev Clin Oncol*. 2019;16(2):81–104.
6. Zhou ZR, Yang ZZ, Yu XL, Guo XM. Highlights on molecular targets for radiosensitization of breast cancer cells: current research status and prospects. *Cancer Med*. 2018;7(7):3110–7.
7. Huang R, Gao S, Han Y, Ning H, Zhou Y, Guan H, et al. BECN1 promotes radiation-induced G2/M arrest through regulation CDK1 activity: a potential role for autophagy in G2/M checkpoint. *Cell Death Discov*. 2020;6(1):1–17.
8. Soleimani V, Sahebkar A, Hosseinzadeh H. Turmeric (*Curcuma longa*) and its major constituent (curcumin) as nontoxic and safe substances. *Phytother Res*. 2018;32(6):985–95.
9. Sharifi-Rad J, Rayess YE, Rizk AA, Sadaka C, Zgheib R, Zam W, et al. Turmeric and its major compound curcumin on health: bioactive effects and safety profiles for food, pharmaceutical, biotechnological and medicinal applications. *Front Pharmacol*. 2020;11:1021.
10. Adiwidjaja J, McLachlan AJ, Boddy AV. Curcumin as a clinically-promising anti-cancer agent: pharmacokinetics and drug interactions. *Expert Opin Drug Metab Toxicol*. 2017;13(8):953–72.
11. Farhood B, Mortezaee K, Goradel NH, Khanlarkhani N, Salehi E, Nashtaei MS, et al. Curcumin as an anti-inflammatory agent: Implications to radiotherapy and chemotherapy. *J Cell Physiol*. 2019;234(5):5728–40.
12. Shen L, Liu C-C, An C-Y, Ji H-F. How does curcumin work with poor bioavailability? Clues from experimental and theoretical studies. *Sci Rep*. 2016;6(1):1–10.
13. Tan BL, Norhaizan ME. Curcumin combination chemotherapy: The implication and efficacy in cancer. *Molecules*. 2019;24(14):2527.
14. Flora G, Gupta D, Tiwari A. Nanocurcumin: a promising therapeutic advancement over native curcumin. *Crit Rev Ther Drug Carrier Syst*. 2013;30:4.
15. Moniruzzaman M, Min T. Curcumin, curcumin nanoparticles and curcumin nanospheres: a review on their pharmacodynamics based on monogastric farm animal, poultry and fish nutrition. *Pharmaceutics*. 2020;12(5):447.
16. Prasad S, Tyagi AK, Aggarwal BB. Recent developments in delivery, bioavailability, absorption and metabolism of curcumin: the golden pigment from golden spice. *Cancer Res Treat*. 2014;46(1):2.
17. Naksuriya O, Okonogi S, Schifflers RM, Hennink WE. Curcumin nanoformulations: a review of pharmaceutical properties and preclinical studies and clinical data related to cancer treatment. *Biomaterials*. 2014;35(10):3365–83.
18. Sarbolouki MN, Sadeghizadeh M, Yaghoobi MM, Karami A, Lohrasbi T. Dendrosomes: a novel family of vehicles for transfection and therapy. *J Chem Technol Biotechnol*. 2000;75(10):919–22.
19. Sadeghizadeh M, Ranjbar B, Damaghi M, Khaki L, Sarbolouki MN, Najafi F, et al. Dendrosomes as novel gene porters-III. *J Chem Technol Biotechnol*. 2008;83(6):912–20.
20. Babaei E, Sadeghizadeh M, Hassan ZM, Feizi MAH, Najafi F, Hashemi SM. Dendrosomal curcumin significantly suppresses cancer cell proliferation in vitro and in vivo. *Int Immunopharmacol*. 2012;12(1):226–34.
21. Tahmasebi Mirgani M, Isacchi BSM, Marra F, Bilia AR, Mowla SJ, Najafi F, et al. Dendrosomal curcumin nanoformulation downregulates pluripotency genes via miR-145 activation in U87MG glioblastoma cells. *Int J Nanomed*. 2014;9(1):403–17.
22. Farhangi B, Alizadeh AM, Khodayari H, Khodayari S, Dehghan MJ, Khori V, et al. Protective effects of dendrosomal curcumin on an animal metastatic breast tumor. *Eur J Pharmacol*. 2015;758:188–96.
23. Zamani M, Sadeghizadeh M, Behmanesh M, Najafi F. Dendrosomal curcumin increases expression of the long non-coding RNA gene MEG3 via up-regulation of epi-miRs in hepatocellular cancer. *Phytomedicine*. 2015;22(10):961–7.
24. Montazeri M, Sadeghizadeh M, Pilehvar-Soltanahmadi Y, Zarghami F, Khodi S, Mohaghegh M, et al. Dendrosomal curcumin nanoformulation modulate apoptosis-related genes and protein expression in hepatocarcinoma cell lines. *Int J Pharm*. 2016;509(1–2):244–54.
25. Eslami SS, Jafari D, Montazeri H, Sadeghizadeh M, Tarighi P. Combination of curcumin and metformin inhibits cell growth and induces apoptosis without affecting the cell cycle in LNCaP prostate cancer cell line. *Nutr Cancer*. 2021;73(6):1026–39.
26. Pakizehkar S, Ranji N, Naderi Sohi A, Sadeghizadeh M. Curcumin loaded PEG400-OA nanoparticles: a suitable system to increase apoptosis, decrease migration, and deregulate miR-125b/miR182 in MDA-MB-231 human breast cancer cells. *Polym Adv Technol*. 2020;31(8):1793–804.
27. Djalali M, Djalali M, Abdolahi M, Mohammadi H, Heidari H, Hosseini S, et al. The effect of nano-curcumin supplementation on pentraxin 3 gene expression and serum level in migraine patients. *Rep Biochem Mol Biol*. 2020;9(1):1.
28. Yin N, Xie T, Zhang H, Chen J, Yu J, Liu F. IDH1-R132H mutation radiosensitizes U87MG glioma cells via epigenetic down-regulation of TIGAR. *Oncol Lett*. 2020;19(2):1322–30.
29. Zhou Z-R, Wang X-Y, Yu X-L, Mei X, Chen X-X, Hu Q-C, et al. Building radiation-resistant model in triple-negative breast cancer to screen radioresistance-related molecular markers. *Ann Transl Med*. 2020;8:4.
30. Riss TL, Moravec RA, Niles AL, Duellman S, Benink HA, Worzella TJ, et al. Cell viability assays. *Assay Guidance Manual* [Internet]. 2016.
31. Kunwar A, Barik A, Mishra B, Rathinasamy K, Pandey R, Priyadarsini K. Quantitative cellular uptake, localization and cytotoxicity of curcumin in normal and tumor cells. *Biochim Biophys Acta Gen Subj*. 2008;1780(4):673–9.
32. Franken NA, Rodermond HM, Stap J, Haveman J, Van Bree C. Clonogenic assay of cells in vitro. *Nat Protoc*. 2006;1(5):2315–9.
33. Lim KJ, Bisht S, Bar EE, Maitra A, Eberhart CG. A polymeric nanoparticle formulation of curcumin inhibits growth, clonogenicity and stem-like fraction in malignant brain tumors. *Cancer Biol Ther*. 2011;11(5):464–73.
34. Fried J, Perez AG, Clarkson BD. Flow cytometric analysis of cell cycle distributions using propidium iodide. Properties of the method and mathematical analysis of the data. *J Cell Biol*. 1976;71(1):172–81.
35. Vermes I, Haanen C, Steffens-Nakken H, Reutelingsperger C. A novel assay for apoptosis flow cytometric detection of phosphatidylserine expression on early apoptotic cells using fluorescein labelled annexin V. *J Immunol Methods*. 1995;184(1):39–51.
36. Ribble D, Goldstein NB, Norris DA, Shellman YG. A simple technique for quantifying apoptosis in 96-well plates. *BMC Biotechnol*. 2005;5(1):1–7.
37. Schneider CA, Rasband WS, Eliceiri KW. NIH Image to ImageJ: 25 years of image analysis. *Nat Methods*. 2012;9(7):671–5.
38. Cummings BS, Schnellmann RG. Measurement of cell death in mammalian cells. *Curr Protoc Pharmacol*. 2004;25(1):1–22.
39. Kravtsov V, Livanova A, Starkova Y. Nuclear abnormalities of lymphocytes as the simplest markers for bioindication test in case of mass casualty events involving radiation exposure. *Emerg Med (Los Angel)*. 2017;7(356):2.

40. Livak KJ, Schmittgen TD. Analysis of relative gene expression data using real-time quantitative PCR and the 2- $\Delta\Delta$ CT method. *Methods*. 2001;25(4):402–8.
41. Braselmann H, Michna A, Heß J, Unger K. CFAssay: statistical analysis of the colony formation assay. *Radiat Oncol*. 2015;10(1):1–6.
42. Cichoń M. Reporting statistical methods and outcome of statistical analyses in research articles. *Pharmacol Rep*. 2020;72(3):481–5.
43. Carlson DJ, Stewart RD, Li XA, Jennings K, Wang JZ, Guerrero M. Comparison of in vitro and in vivo  $\alpha/\beta$  ratios for prostate cancer. *Phys Med Biol*. 2004;49(19):4477.
44. McMahon SJ. The linear quadratic model: usage, interpretation and challenges. *Phys Med Biol*. 2018;64(1):1.
45. Kim IA, Kim JH, Shin JH, Kim IH, Kim JS, Wu H-G, et al. A histone deacetylase inhibitor, trichostatin A, enhances radiosensitivity by abrogating G2/M arrest in human carcinoma cells. *Cancer Res Treat*. 2005;37(2):122.
46. Valeriote F, Lin H-S. Synergistic interaction of anticancer agents: a cellular perspective. *Cancer Chemother Rep*. 1975;59(5):895–900.
47. Carpentier Y, Demange L, Loirette M, Hivet J, Desoize B. Chronology of combined chemotherapy (5FU) and radiotherapy I In vitro study. *Anticancer Res*. 1993;13(6A):2177–80.
48. Sak K. Radiosensitizing potential of curcumin in different cancer models. *Nutr Cancer*. 2020;72(8):1276–89.
49. Hosseini A, Hosseinzadeh H. Antidotal or protective effects of *Curcuma longa* (turmeric) and its active ingredient, curcumin, against natural and chemical toxicities: a review. *Biomed Pharmacother*. 2018;99:411–21.
50. Reuter S, Eifes S, Dicato M, Aggarwal BB, Diederich M. Modulation of anti-apoptotic and survival pathways by curcumin as a strategy to induce apoptosis in cancer cells. *Biochem Pharmacol*. 2008;76(11):1340–51.
51. Kesari S, Advani SJ, Lawson JD, Kahle KT, Ng K, Carter B, et al. DNA damage response and repair: insights into strategies for radiation sensitization of gliomas. *Future Oncol*. 2011;7(11):1335–46.
52. Ahmed KM, Li JJ. NF- $\kappa$ B-mediated adaptive resistance to ionizing radiation. *Free Radic Biol Med*. 2008;44(1):1–13.
53. Graham K, Unger E. Overcoming tumor hypoxia as a barrier to radiotherapy, chemotherapy and immunotherapy in cancer treatment. *Int J Nanomedicine*. 2018;13:6049.
54. Szczerba BM, Castro-Giner F, Vetter M, Krol I, Gkountela S, Landin J, et al. Neutrophils escort circulating tumour cells to enable cell cycle progression. *Nature*. 2019;566(7745):553–7.
55. Soltani B, Bodaghabadi N, Mahpour G, Ghaemi N, Sadeghizadeh M. Nanoformulation of curcumin protects HUVEC endothelial cells against ionizing radiation and suppresses their adhesion to monocytes: potential in prevention of radiation-induced atherosclerosis. *Biotechnol Lett*. 2016;38(12):2081–8.
56. Soltani B, Ghaemi N, Sadeghizadeh M, Najafi F. Curcumin confers protection to irradiated THP-1 cells while its nanoformulation sensitizes these cells via apoptosis induction. *Cell Biol Toxicol*. 2016;32(6):543–61.
57. Yallapu MM, Jaggi M, Chauhan SC. Curcumin nanoformulations: a future nanomedicine for cancer. *Drug Discov Today*. 2012;17(1–2):71–80.
58. Kim S, An SSA. Role of p53 isoforms and aggregations in cancer. *Medicine*. 2016;95:26.
59. Cheng C, Jiao JT, Qian Y, Guo XY, Huang J, Dai MC, et al. Curcumin induces G2/M arrest and triggers apoptosis via FoxO1 signaling in U87 human glioma cells. *Mol Med Rep*. 2016;13(5):3763–70.
60. Bagherian A, Mardani R, Roudi B, Taghizadeh M, Banfshe HR, Ghaderi A, et al. Combination therapy with nanomicellar-curcumin and temozolomide for in vitro therapy of glioblastoma multiforme via Wnt signaling pathways. *J Mol Neurosci*. 2020;70(10):1471–83.
61. Aoki H, Takada Y, Kondo S, Sawaya R, Aggarwal BB, Kondo Y. Evidence that curcumin suppresses the growth of malignant gliomas in vitro and in vivo through induction of autophagy: role of Akt and extracellular signal-regulated kinase signaling pathways. *Mol Pharmacol*. 2007;72(1):29–39.
62. Zhao J, Zhu J, Lv X, Xing J, Liu S, Chen C, et al. Curcumin potentiates the potent antitumor activity of ACNU against glioblastoma by suppressing the PI3K/AKT and NF- $\kappa$ B/COX-2 signaling pathways. *Onco Targets Ther*. 2017;10:5471.
63. Qian Y, Ma J, Guo X, Sun J, Yu Y, Cao B, et al. Curcumin enhances the radiosensitivity of U87 cells by inducing DUSP-2 up-regulation. *Cell Physiol Biochem*. 2015;35(4):1381–94.
64. Luthra PM, Kumar R, Prakash A. Demethoxycurcumin induces Bcl-2 mediated G2/M arrest and apoptosis in human glioma U87 cells. *Biochem Biophys Res Commun*. 2009;384(4):420–5.
65. Hackler L Jr, Ózsvári B, Gyuris M, Sipos P, Fábrián G, Molnár E, et al. The curcumin analog C-150, influencing NF- $\kappa$ B, UPR and Akt/Notch pathways has potent anticancer activity in vitro and in vivo. *PLoS ONE*. 2016;11(3): e0149832.
66. Du WZ, Feng Y, Wang XF, Piao XY, Cui YQ, Chen LC, et al. Curcumin suppresses malignant glioma cells growth and induces apoptosis by inhibition of SHH/GLI 1 signaling pathway in vitro and vivo. *CNS Neurosci Ther*. 2013;19(12):926–36.
67. Guan F, Ding Y, Zhang Y, Zhou Y, Li M, Wang C. Curcumin suppresses proliferation and migration of MDA-MB-231 breast cancer cells through autophagy-dependent Akt degradation. *PLoS ONE*. 2016;11(1): e0146553.
68. Sun X-D, Liu X-E, Huang D-S. Curcumin induces apoptosis of triple-negative breast cancer cells by inhibition of EGFR expression. *Mol Med Rep*. 2012;6(6):1267–70.
69. Zhou X, Jiao D, Dou M, Zhang W, Lv L, Chen J, et al. Curcumin inhibits the growth of triple-negative breast cancer cells by silencing EZH2 and restoring DLC1 expression. *J Cell Mol Med*. 2020;24(18):10648–62.
70. Hu S, Xu Y, Meng L, Huang L, Sun H. Curcumin inhibits proliferation and promotes apoptosis of breast cancer cells. *Exp Ther Med*. 2018;16(2):1266–72.
71. Bimonte S, Barbieri A, Palma G, Rea D, Luciano A, D'Aiuto M, et al. Dissecting the role of curcumin in tumour growth and angiogenesis in mouse model of human breast cancer. *Biomed Res Int*. 2015;2015: 878134.
72. Sun S-H, Huang H-C, Huang C, Lin J-K. Cycle arrest and apoptosis in MDA-MB-231/Her2 cells induced by curcumin. *Eur J Pharmacol*. 2012;690(1–3):22–30.
73. Moghtaderi H, Sepehri H, Delphi L, Attari F. Gallic acid and curcumin induce cytotoxicity and apoptosis in human breast cancer cell MDA-MB-231. *BioImpacts*. 2018;8(3):185.
74. Stepulak A, Sifringer M, Rzeski W, Endesfelder S, Gratopp A, Pohl EE, et al. NMDA antagonist inhibits the extracellular signal-regulated kinase pathway and suppresses cancer growth. *Proc Natl Acad Sci*. 2005;102(43):15605–10.
75. Macleod KF, Sherry N, Hannon G, Beach D, Tokino T, Kinzler K, et al. p53-dependent and independent expression of p21 during cell growth, differentiation, and DNA damage. *Genes Dev*. 1995;9(8):935–44.
76. Liu Z-B, Zhang T, Ye X, Liu Z-Q, Sun X, Zhang L-L, et al. Natural substances derived from herbs or plants are promising sources of anticancer agents against colorectal cancer via triggering apoptosis. *J Pharm Pharmacol*. 2022;74(2):162–78.
77. Mukhopadhyay A, Banerjee S, Stafford LJ, Xia C, Liu M, Aggarwal BB. Curcumin-induced suppression of cell proliferation correlates with down-regulation of cyclin D1 expression and CDK4-mediated retinoblastoma protein phosphorylation. *Oncogene*. 2002;21(57):8852–61.

78. Su C-C, Lin J-G, Chen G-W, Lin W-C, Chung J-G. Down-regulation of Cdc25c, CDK1 and Cyclin B1 and up-regulation of Wee1 by curcumin promotes human colon cancer Colo 205 cell entry into G2/M-phase of cell cycle. *Cancer Genom Proteom.* 2006;3(1):55–61.
79. Patil SL, Swaroop K, Kakde N, Somashekarappa H. In vitro protective effect of rutin and quercetin against radiation-induced genetic damage in human lymphocytes. *Indian J Nucl Med.* 2017;32(4):289.
80. Kravtsov VY, Fedortseva R, Starkova YV, Yartseva N, Nikiforov A. Tailed nuclei and dicentric chromosomes in irradiated subjects. *Appl Radiat Isot.* 2000;52(5):1121–7.

**Publisher's Note** Springer Nature remains neutral with regard to jurisdictional claims in published maps and institutional affiliations.